



Nonlinear multiscale Maximal Lyapunov Exponent for accurate myoelectric signal classification



Yina Guo^a, Ganesh R. Naik^{b,*}, Shuhua Huang^a, Ajith Abraham^c, Hung T. Nguyen^b

^a Taiyuan University of Science and Technology, Taiyuan 030024, Shanxi, China

^b Centre for Health Technologies (CHT), University of Technology, Sydney 2007, Australia

^c Machine Intelligence Research Labs (MIR Labs), Scientific Network for Innovation and Research Excellence, P.O. Box 2259, Auburn, WA 98071-2259, USA

ARTICLE INFO

Article history:

Received 7 May 2014

Received in revised form 1 April 2015

Accepted 27 July 2015

Available online 10 August 2015

Keywords:

Empirical Mode Decomposition (EMD)

Flexible Neural Trees (FNT)

Hand gesture recognition

Maximal Lyapunov Exponent (MLE)

Principal Component Analysis (PCA)

Surface Electromyography (sEMG)

ABSTRACT

Surface Electromyography (sEMG) is a non-invasive, easy to record signal of superficial muscles from the skin surface. The sEMG is widely used in evaluating the functional status of the hand to assist in hand gesture recognition, prosthetics and rehabilitation applications. Considering the nonlinear and non-stationary characteristics of sEMG, hand gesture recognition using sEMG signals necessitate designers to use Maximal Lyapunov Exponent (MLE) or ensemble Empirical Mode Decomposition (EMD) based MLEs. In this research, we propose a hand gesture recognition method of sEMG based on nonlinear multiscale MLE. The aim is to increase the classification accuracy of sEMG features while reducing the complexity of EMD. The nonlinear MLE features are classified using Flexible Neural Tree (FNT), which can solve highly structured dependent problems of the Artificial Neural Network (ANN). The testing has been conducted using several experiments with five participants. The classification performance of nonlinear multiscale MLE method is compared with MLE and EMD-based MLE through simulations. Experimental results demonstrate that the former algorithm outperforms the two latter algorithms and can classify six different hand gestures up to 97.6% accuracy.

© 2015 Elsevier B.V. All rights reserved.

1. Introduction

Over the years, Myoelectric Control Systems (MCSs) have been extensively used for controlling assistive and rehabilitation devices by conducting the classified patterns of Surface Electromyography (sEMG) signals [1]. Surface EMG also known as myoelectric signal is an electrical potential which is generated by the muscle cells when these cells are electrically or neurologically activated [2]. It is detected from superficial muscles by using surface electrodes and deep layer muscles by using needle electrodes. The sEMG has various applications, for instance, doctors in hospital use sEMG for the diagnosis of neurological and neuromuscular problems, biomedical engineers use sEMG as a control signal for prosthetic devices including prosthetic hands, arms, lower limbs and intelligent wheelchairs. Also, sEMG has been widely used to detect medical abnormalities, activation level, and recruitment pattern to analyze the biomechanics of human or animal movement [1].

In the biomedical research community, it is a well-known phenomenon that interference and cross-talk introduces non-linearity into the biomedical signals [3,4]. Most of the existing techniques used for sEMG feature extraction are generally based on the linearity of the signal; however, sometimes, this assumption may be compromised due to cross-talk and interference from the adjacent muscles. Moreover, the sEMG signal is extremely complex as it is influenced by several factors in the electrophysiology and the recording environment [3,4]. Numerous research studies have been conducted to investigate the complexity and non-linear nature of sEMG signals. Meng and Liu [5] studied the nonlinear determinacy of sEMG signals and concluded that EMG obeys a certain non-linear and chaos characteristics within the signal. Padmanabhan and Puthusserypaday [4] explored nonlinear chaotic method to study the nonlinear characteristics of sEMG signals, including correlation dimension, Lyapunov spectrum, Kaplan–Yorke dimension and recurrence plots. In a more recent study Ai et al. [6] have used Local Lyapunov Exponent (LLE) and Artificial Neural Network (ANN) to classify six different gestures. Although the results are satisfactory, the method suffers from issues such as training of data and classification errors.

Non-linear time series methods such as phase-space reconstruction, chaotic characterization, non-linear prediction and Maximal

* Corresponding author at: University of Technology Sydney, P.O. Box 123, Broadway, NSW 2007, Australia. Tel.: +61 2 9514 4502; fax: +61 2 9514 1810.

E-mail address: Ganesh.Naik@uts.edu.au (G.R. Naik).

Lyapunov Exponent (MLE) have not been used widely with sEMG signals. The MLE is based on a phase space, a construct which demonstrates the changes of the dynamical variables of the system. The sensitivity of a dynamical system to small problems can be quantified by MLE, which exemplifies the average rate of discrepancy in pseudo-periodic practices [7]. Although MLE is capable of modeling the local stability of the nonlinear system in space by analyzing the time-dependent behavior of kinematic variance about a target trajectory, some inherent defects still exist [8,9]. The MLE based methods including LLE, Wolf Lyapunov Exponent (WLE), Rosenstein Lyapunov Exponent (RLE), Kantz Lyapunov Exponent (KLE) and Ensemble Empirical Mode Decomposition (EEMD) based MLE are usually employed in biomechanics and human movement science [8]. LLE has high sensitivity to initial conditions and noise, whereas WLE, RLE and KLE are not easily affected by topology complexity and have certain anti-interference ability. However, WLE is susceptible to multi-parameter situations and requires a long data length [10]. Moreover, none of the above mentioned MLE methods can recognize the multiscale characteristic of fractional Brownian motion [3]. On the other hand, Empirical Mode Decomposition (EMD) based MLE method possesses the recognition ability of multiscale characteristic in fractional Brownian motion and has demonstrated higher sEMG classification accuracy [11]. But EMD based decomposition techniques have drawbacks, such as multiple dimensions, which cannot be reduced automatically [12].

This research proposes a new technique based on nonlinear multiscale MLE. The motivation to use the nonlinear multiscale MLE for sEMG analysis is due to its ability to estimate the amount of chaos in a system. The nonlinear multiscale MLE differs from the traditional MLE or EMD – based MLE by more accurate and reliable recognition measurements of seems signals, more simplified EMD decomposition process and Intrinsic Mode Functions (IMFs) dimension reduction process.

In this research, sEMG features were extracted using nonlinear multiscale MLE, and classified using Flexible Neural Tree (FNT). The advantage of using FNT is that it can solve structure dependent problem of the ANN. The recognition performance of the proposed nonlinear multiscale MLE myoelectric scheme is also compared with MLE and EMD-based MLE via simulations. The rest of the paper is organized as follows: the EMD, PCA, MLE and FNT principles are briefly summarized in the first part of the paper. The method, feature extraction and selection are then explained in detail. The classification and evaluation of the proposed method are explained in the third part. Final part of the paper discusses the outcome of the proposed research and discusses about future directions of the research.

2. Theory

In order to explain the concept of NMMLE method, first of all it is imperative to briefly highlight the fundamental theory of MLE.

2.1. Empirical Mode Decomposition (EMD)

EMD is a single-channel technique that decomposes any complicated time series data into a finite set of oscillatory modes called IMFs, and obtains instantaneous frequency data. EMD is the fundamental part of the Hilbert–Huang Transform (HHT), which was proposed by Huang et al. [13]. The definition of an IMF guarantees a well-behaved Hilbert transform of the IMF. This decomposition method operating in the time domain is adaptive and highly efficient. Since the decomposition is based on the local characteristic time scale of the data, it can be applied to both nonlinear and non-stationary processes.

2.2. Principal Component Analysis (PCA)

PCA is one of the widely used dimensional reduction technique. It is a mathematical procedure that uses an orthogonal transformation to convert a set of observations of possibly correlated variables X into a set of values of uncorrelated variables Y called Principal Components (PCs). PCs are guaranteed to be independent only if the data set is jointly or normally distributed. If a multivariate dataset is visualized as a set of coordinates in a high-dimensional data space (1 axis per variable), PCA can supply the user with a lower-dimensional picture and this is done by using only the first few PCs so that the dimensionality of the transformed data is reduced [14,15].

2.3. Maximal Lyapunov Exponent (MLE)

In mathematics the Lyapunov exponent of a dynamical system is a quantity that characterizes the rate of separation of infinitesimally close trajectories. In general, spectrum of Lyapunov exponents is equal in number to the dimensionality of the phase space. The largest among them is the MLE, which determines a notion of predictability for a dynamical system. Because of the exponential growth rate, the effect of the other exponents (Lyapunov exponents) will be eliminated over time, and hence, the MLE does not use the Lyapunov method. The MLE is generally used for machine fault diagnosis, physiological rhythm measurement, muscle contraction and muscle activity detection. MLE can be defined as follows [16]:

$$\lambda = \lim_{t \rightarrow \infty} \lim_{\delta Z_0 \rightarrow 0} \frac{1}{t} \ln \frac{|\delta Z(t)|}{|\delta Z_0|} \quad (1)$$

where δZ_0 represents the initial separation and the limit $\delta Z_0 \rightarrow 0$ ensures the validity of the linear approximation at any time.

A nearest neighbor based method for estimating the largest Lyapunov exponent was proposed by Sato et al. [17]. The calculation of this algorithm is simple and is similar to WOLF algorithm. The MLEs of the whole set of IMFs can be obtained by using SATO's method, where the distance of the adjacent orbits has typically multiplied by forecasting error on a log scale [18]. It can be defined as:

$$p(k) = \frac{1}{NT_s} \sum_{n=1}^N 1b \frac{||X_{n+k} - X_{nn+k}||}{||X_n - X_{nn}||} \quad (2)$$

where T_s is a sample period which can be obtained by Fast Fourier Transform (FFT) algorithm. N is the amount of phase points. In the path of phase space, $||X_n - X_{nn}||$ is the distance between X_{nn} and X_n . X_{nn} is the nearest point from X_n . $||X_{n+k} - X_{nn+k}||$ represents the distance between X_{nn} and X_n which is after k evolutionary step length. In the $p(k) - k$ graph line, the slope of straight line is MLE.

2.4. Flexible Neural Trees

The FNT is a fuzzy model which was proposed mainly for solving highly structure dependent problems of the ANN. The FNT has been applied in many areas such as face recognition and microarray-based cancer classification [19]. In comparing models for the non-linear function approximation, it has lower Mean Square Error (MSE) than back-propagation and fuzzy clustering techniques [19–21]. The function instruction operators F and instruction terminals T used for evolving a FNT model with instruction set S are described as:

$$S = F \cup T = \{+2, +3, \dots, +N\} \cup \{x_1, x_2, \dots, x_n\} \quad (3)$$

where $+i$ ($i = 2, 3, \dots, N$) denote instructions of non-leaf nodes which take i arguments, \cup represents joining function (joins F and T), and x_1, x_2, \dots, x_n represent instructions of leaf nodes which take

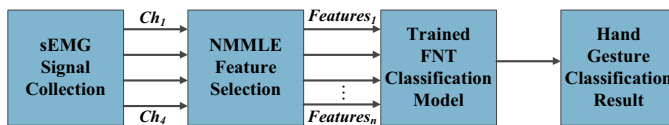


Fig. 1. The structure of hand gesture recognition model.

no other arguments. It is shown clearly that the output of a non-leaf node $+_n$, which is also known as a flexible neuron operator, is calculated as a flexible neuron model with n arguments.

In the FNT construction process, when a non-leaf instruction $+_i (i=2, 3, \dots, N)$ is selected, i real values are evolved automatically and used for demonstrating the connection strength between the node $+_i$ and its children. The output of a flexible neuron $+_n$ can be calculated as:

$$net_n = \sum_{j=1}^n \omega_j x_j \quad (4)$$

where $x_j (j=1, 2, \dots, n)$ are the inputs to node $+_n$ and ω_j is the weight connection between x_j and $+_n$

In flexible activation function $f(a_i, b_i, x)$, two adjustable parameters a_i and b_i are randomly created as flexible activation function parameters. When flexible activation function is determined, the output of the node $+_n$ is calculated by:

$$out_n = f(a_n, b_n, net_n) = e^{-(x-a_n)/b_n} \quad (5)$$

where a_n and b_n the parameters are adjustable parameters. The FNT model can be created and evolved using the existing or modified tree-structure-based approaches, which include Probabilistic Incremental Program Evolution (PIPE) and Ant Programming (AP). Normally, the fitness function used for the PIPE and Simulated Annealing (SA) can be given by Mean Square Error (MSE) or Root Mean Square Error (RMSE). The FNT model is computed as an irregular flexible multi-layer feed-forward neural network. Based on the pre-defined instruction/operator sets, a flexible neural tree can be created and evolved. In this approach, over-layer connections, different activation functions for different nodes and input variables selection are allowed.

The proposed method incorporates both optimization techniques. Starting with random structures and corresponding parameters, it first tries to improve the structure and then as soon as an improved configuration is found, it fine tunes its parameters. It then goes back to improve the structure again and fine tunes the configuration and rules' parameters. This loop continues until a satisfactory solution is found or a time limit is reached. The FNT model works well for generating an approximating model of the static non-linear system [22,23].

3. Methodology

Experiments were conducted to evaluate the performance of the proposed sEMG based isometric hand gesture recognition system. The main objective of the signal collection, feature selection, and classification is to design and develop a robust classification scheme for naturally controlled myoelectric prosthetic hand. In order to classify different hand gestures efficiently, the overall classification scheme involve myoelectric signal collection, important/significant feature selection, and classification of appropriate gestures. The schematics diagram of the proposed myoelectric signal classification scheme is shown in Fig. 1, which consists of sEMG signal collection, feature selection/extraction, FNT classification and hand gesture recognition parts. Feature selection section takes the responsibilities for selecting and computing sEMG features by the use of NMMLE. In FNT classification section, the FNT is adopted

to train a fuzzy classification model according to the selected sEMG features and the initialization construction. The trained classification model is applied for testing the accuracy of the hand gesture recognition system.

3.1. sEMG signal collection

For the hand gesture experiments five subjects, four males and one female, aged 26 ± 5.8 , height 1.6 ± 0.12 m and weight 55 ± 7.2 kg were chosen. All volunteers are healthy, with no history of muscle weakness and neurological diseases. The volunteers have approved and signed an informed consent form, according to the experiments to be performed. The sEMG data were recorded via our own sEMG signal acquisition equipment with the necessary protection circuit (see Fig. 2). A signal conditioning circuit was designed for each channel with high input impedance instrumentation amplifier. A high pass filter of 10 Hz cut-off frequency was connected after the instrumentation amplifier to prevent DC voltage offsets caused by skin impedance and reaction between the skin and electrode gel. Further, the circuitry was designed to have output from the high pass filter and variable gain amplifier (gain 6–100) and to band pass filter of 10–500 Hz to obtain signals in a dominant energy band. Each channel has a fixed inter-electrode distance of 10 mm, a gain of 1000 and common mode rejection ratio of 104 dB. Based on the finger and wrist movement tasks and the muscle anatomy of human upper limbs, several forearm muscles can contribute to the designed multi-finger movements [2]. Through a large number of preliminary experiments, we identified four forearm muscles as suitable candidates for the designed recognition problem of hand gestures. Four electrode channels were placed over four different muscles as indicated in Table 1 and Fig. 2. The electrodes were connected via adhesive medical tapes. A reference electrode was placed at Epicondylus Medialis.

Before placing the electrodes, the subject's skin was prepared by lightly abrading with skin exfoliate to remove dead skin that helps in reducing the skin impedance to less than $60 \text{ k}\Omega$. The skin was also cleaned with 70% (v/v) alcohol swab to remove any oil or dust on the skin surface. To find corresponding muscles correctly, we asked the subjects to perform certain hand actions suggested by an expert in the field.

Subjects were asked to keep the forearm resting on the table with elbow at an angle of 90 degrees in a comfortable position. The order of the flexions is arbitrary and each flexion is maintained for about 10 s to record sEMG and the duration of each run of the experiment was about 60 s. Each time raw signal sampled at 1024 samples/s was recorded. Markers were used to obtain the hand and finger contraction signals during recording. A suitable resting time was given between each experiment. There was no external load. The actions were complex to determine the ability of the system when similar muscles were active simultaneously. The six different hand actions were performed and they are: (i) ring finger flexion, (ii) index finger flexion, (iii) middle finger flexion, (iv) thumb finger flexion, (v) all finger flexion and (vi) wrist flexion. These hand actions were selected based on small variations between the muscle activities of the different digits muscles situated in the forearm.

3.2. Feature selection for NMMLE method

Five volunteers participated in the experiments. Each participant performed one kind of flexion for 6 times for each of the 6 designed finger and wrist movements. Hence, there were totally 30 trials for each movement in the defined number gesture movement set. Prior to feature extraction, movement artifact (<20 Hz), power-line interference (50 Hz) and high-frequency noise (>450 Hz) were removed. The recorded sEMG data were divided into overlapping windows of 256 ms length with a 64 ms increment

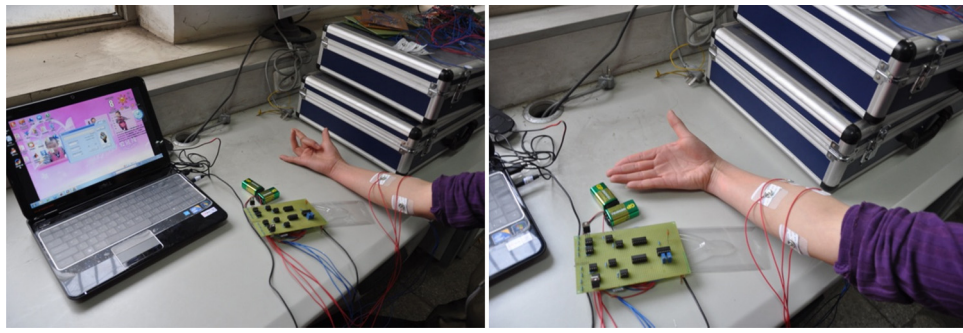


Fig. 2. Circuit used for sEMG signal collection.

Table 1

Muscle anatomy for the placement of electrodes over the skin of the forearm.

Channel	Muscle	Function
1	Brachioradialis	Flexion of forearm
2	Flexor Digitorum Superficialis (FDS)	Finger flexion while avoiding wrist flexion
3	Flexor Carpi Radialis (FCR)	Abduction and flexion of wrist
4	Flexor Carpi Ulnaris (FCU)	Abduction and flexion of wrist

(25% overlapping) between windows. This segmentation scheme was used for all numerical experiments in this study. Surface EMG features such as Delay time and Embedding Dimension were calculated for each channel separately. Both Delay time and Embedding Dimension are two important parameters used for calculating Lyapunov exponent. These are also particularly well suited for the representation of dynamic behavior of sEMG gesture time series data for a very pragmatical reason – they tend to have shorter motor unit bursts, in the sense that for each gesture movement window the number of allowed time points is typically 256 ms, in the sense that the controller delay is compensated. Moreover, these two parameters are chosen properly to determine the sEMG signal motion characteristics.

3.2.1. Delay time

The delay time τ is determined by using mutual information method. It is defined as:

$$I(\tau) = \sum_{n=1}^N p(Y_n, Y_{n+\tau}) \ln \frac{p(Y_n, Y_{n+\tau})}{p(Y_n)p(Y_{n+\tau})} \quad (6)$$

where $p(Y_n), p(Y_{n+\tau}), p(Y_n, Y_{n+\tau})$ are probability values. In the $I(\tau) - \tau$ graph line, the value of the first minimum point corresponds to delay time τ .

3.2.2. Embedding dimension

In this research study, we use improved pseudo neighbor method to calculate embedding dimension d [24]. This method does not require a subjective parameter and is adapted to a high dimensional dynamical system and the situation of minimum data. In addition, it can distinguish the random and determinate signals. The embedding dimension $E_1(d)$ is calculated as:

$$E_1(d) = \frac{E(d+1)}{E(d)} \quad (7)$$

where $E(d)$ and $E(d+1)$ are the mean threshold values of all of the two nearest neighbors' distance in the reconstruction d dimension space and the reconstruction $d+1$ dimension space respectively. In the $E_1(d) - d$ graph line, the minimum embedding dimension corresponds to $E_1(d)$ value when $E_1(d)$ value does not change significantly with an increase in d value.

3.2.3. EMD decomposition

After EMD is performed in each channel signal $s(t)$, a set of averaged IMFs c_j (see Eq. (2)) [25] is derived.

$$s(t) = \sum_{j=1}^n c_j + r_n \quad (8)$$

where r_n is the residue of data $s(t)$, after n numbers of IMFs c are extracted. IMFs are simple oscillatory functions with varying amplitude and frequency.

3.2.4. Dimension reduction and MLE

PCA is applied to the whole set of IMFs c to reduce dimensionality. The IMFs are projected down into the reduced space defined by only the first L singular vectors W_L :

$$Y = W_L^T c = \sum_L V^T \quad (9)$$

where $\sum_L = I_{L \times m} \sum$ is an $m \times n$ rectangular diagonal matrix with nonnegative real numbers on the diagonal, and the $n \times n$ matrix V is the matrix of eigenvectors of $c^T c$. After PCA, nonlinear multiscale MLE was employed to get feature vectors for the FNT classifiers. The MLE features were calculated using Eqs. (1) and (2) respectively.

3.3. Hand movement classification by FNT method

In this experiment, the following FNT model is employed to obtain the instruction sets (see Fig. 3).

For developing the FNT classifier, the following flexible activation function is used:

$$f(a_i, b_i, x) = e^{-(x-a_i)/b_i} \quad (10)$$

The output of the node $+_n$ is then calculated by

$$out_n = f(a_n, b_n, net_n) = e^{-(net_n - a_n)/b_n} \quad (11)$$

The PIPE is selected as a tree-structural based encoding method with specific instructions set for fine tuning the parameters encoded in the structure.

A fitness function arranges FNT to scalar and real-valued fitness values that reflect the FNT performances according to a given task.

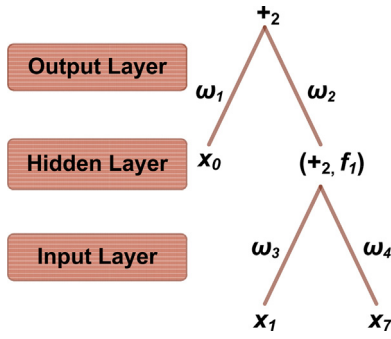


Fig. 3. A flexible neural tree with function instruction sets $I = \{+2, x_0, x_1, x_2, x_3, x_4, x_5, x_6, x_7\}$.

In experiments, the fitness function used for the PIPE is given by RMSE.

$$Fit(i) = \frac{\sum_{j=1}^P (y_1^j - y_2^j)^2}{P} \quad (12)$$

When a satisfactory solution is found or a time limit is reached, the loop stops. The evolved neural tree model is obtained with function instruction sets, $I = \{+2, x_0, x_1, x_2, x_3, x_4, x_5, x_6, x_7\}$.

4. Data analysis

Delay time and embedding dimension are two main parameters of the Lyapunov exponent. If the chosen delay time was too big or too small, the sEMG action could not be optimized. Delay time was determined by using mutual information method. The value of the first minimum point corresponded to delay time is shown in the graph (see Fig. 4).

The minimum embedding dimension $E_1(d)$ corresponded to a value when $E_1(d)$ did not change significantly with an increase in d value. For our sEMG analysis minimum embedding dimension 4 was deemed appropriate (refer Fig. 5).

Considering both the nonlinear and non-stationary characteristic of sEMG, signal was decomposed into a finite set of oscillatory component IMFs. Fig. 6 illustrates the EMD decompositions $c_j(t)$ ($j = 1, \dots, 13$) of the source signal $s_1(t)$. The IMFs $c_j(t)$ ($j = 1, \dots,$

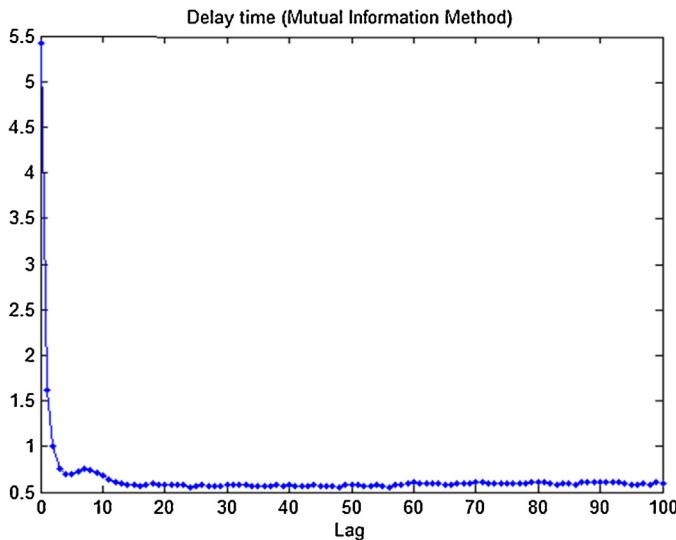


Fig. 4. Delay time of sEMG signal.

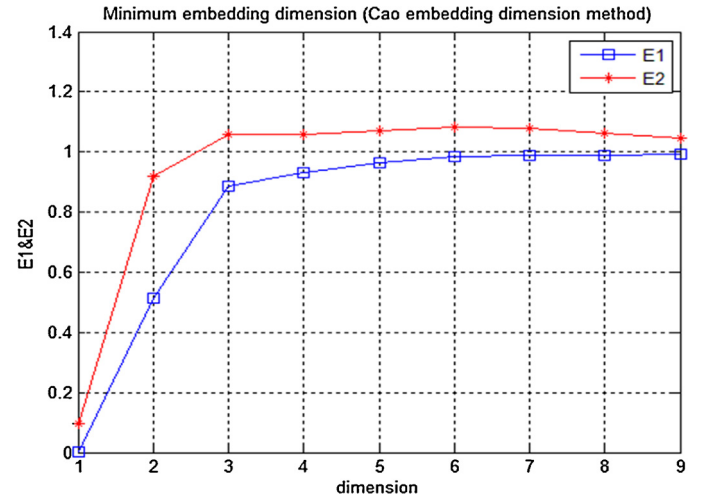


Fig. 5. Minimum embedding dimension of sEMG signal.

13) extracted from $s_1(t)$ were oscillatory functions with varying amplitude and frequency.

From Fig. 6, it can be seen that the IMFs $c_j(t)$ ($j = 5, \dots, 13$) contained very small signal energy, hence the number of IMFs were reduced using PCA. The PCA reduced IMF features are shown in Fig. 7.

As seen in Fig. 7, the eigenvalues of IMFs $c_j(t)$ ($j = 1, \dots, 13$) were mainly concentrated on the first four eigenvalues and therefore selected as features for MLE. After applying PCA to IMFs the average period was computed with the help of Fast Fourier Transform (FFT). The average period was 20. The above calculation parameters, including delay time, embedding dimension and average period, were the main factors of MLE. The MLE of the decomposition IMFs $c_j(t)$ ($j = 1, \dots, 4$) was 0.0820, 0.2394, 0.1452 and 0.0723 respectively (by adopting SATO algorithm).

Finally, FNT was adopted to classify signals and thereby recognized sEMG signal actions. FNT selected proper input variables or time-lags automatically. In addition, the parameters used for FNT data analysis are listed in Table 2. For the experiment, 10 inputs variables were adopted for constructing a FNT model. The instruction set was $I = \{+2, x_0, x_1, x_2, x_3, x_4, x_5, x_6, x_7\}$ (see Fig. 3). For the purpose of testing the hand gesture classification patterns, we sorted the myoelectric features for odd and even numbered

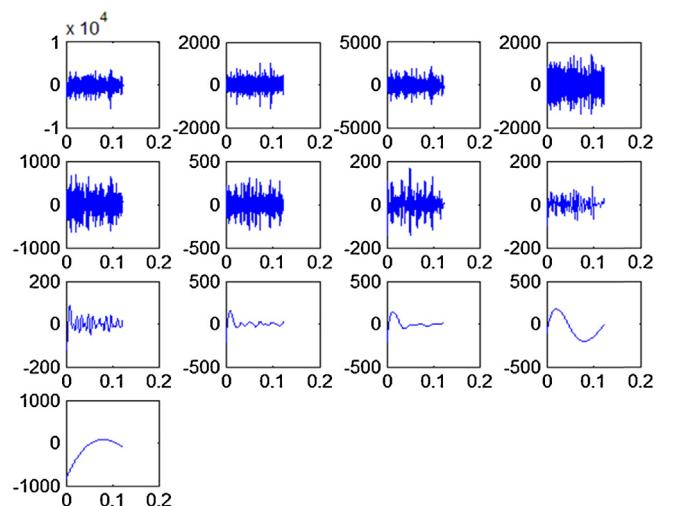


Fig. 6. EMD decomposition of sEMG signal.

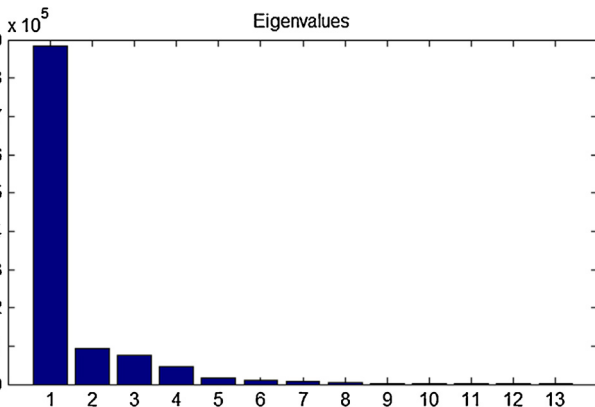


Fig. 7. Eigenvalues of IMFs $c_j(t)$ ($j = 1, \dots, 13$).

trials into training and test sets, respectively. Thus, total 80 trials (5 subjects \times 6 trials \times 6 gestures) yielded 15 training trials and 15 test trials for each gesture. The separation of training and test sets provided a cross-validation of the pattern recognition scheme.

Table 3
The MLEs of original sEMG signals.

Hand gesture	Channel 1 Mean value \pm standard deviation	Channel 2 Mean value \pm standard deviation	Channel 3 Mean value \pm standard deviation	Channel 4 Mean value \pm standard deviation
Ring finger	0.1136 \pm 0.0154	0.2037 \pm 0.0393	0.1828 \pm 0.0168	0.1089 \pm 0.0203
Index finger	0.1161 \pm 0.0171	0.1889 \pm 0.0437	0.1335 \pm 0.021	0.1135 \pm 0.0158
Wrist	0.095 \pm 0.0128	0.1487 \pm 0.019	0.1664 \pm 0.0153	0.0892 \pm 0.0193
Middle finger	0.1248 \pm 0.0175	0.213 \pm 0.0251	0.1962 \pm 0.0727	0.1209 \pm 0.0539
Thumb	0.1227 \pm 0.0202	0.1802 \pm 0.0383	0.197 \pm 0.0204	0.1798 \pm 0.0183
All fingers	0.2098 \pm 0.0602	0.2401 \pm 0.0506	0.2259 \pm 0.014	0.1957 \pm 0.0299

Table 4
The MLE of the decomposition IMFs.

Hand gesture	IMFs	Channel 1 Mean value \pm standard deviation	Channel 2 Mean value \pm standard deviation	Channel 3 Mean value \pm standard deviation	Channel 4 Mean value \pm standard deviation
Ring finger	IMF1	0.1377 \pm 0.0169	0.2506 \pm 0.0223	0.1917 \pm 0.02568	0.1375 \pm 0.0405
	IMF2	0.1244 \pm 0.0232	0.2447 \pm 0.0163	0.1861 \pm 0.025	0.1004 \pm 0.0234
	IMF3	0.1102 \pm 0.043	0.1954 \pm 0.0316	0.1824 \pm 0.0319	0.063 \pm 0.0169
	IMF4	0.0935 \pm 0.0179	0.1977 \pm 0.0232	0.17 \pm 0.0381	0.0555 \pm 0.0139
Index finger	IMF1	0.1211 \pm 0.0226	0.1557 \pm 0.0125	0.1961 \pm 0.0208	0.1483 \pm 0.0376
	IMF2	0.1359 \pm 0.021	0.1883 \pm 0.0197	0.1646 \pm 0.0301	0.0871 \pm 0.0319
	IMF3	0.1262 \pm 0.0148	0.2357 \pm 0.0268	0.1753 \pm 0.0309	0.0921 \pm 0.0325
	IMF4	0.1016 \pm 0.0243	0.1108 \pm 0.0216	0.164 \pm 0.0286	0.0659 \pm 0.0391
Wrist	IMF1	0.1152 \pm 0.018	0.2062 \pm 0.0254	0.1496 \pm 0.0293	0.076 \pm 0.0239
	IMF2	0.1013 \pm 0.0251	0.1014 \pm 0.0253	0.1604 \pm 0.0334	0.0788 \pm 0.0191
	IMF3	0.0939 \pm 0.0211	0.1487 \pm 0.025	0.1352 \pm 0.0184	0.0597 \pm 0.0382
	IMF4	0.0767 \pm 0.0349	0.1443 \pm 0.0232	0.1455 \pm 0.0195	0.071 \pm 0.0291
Middle finger	IMF1	0.1597 \pm 0.0362	0.2583 \pm 0.0568	0.2057 \pm 0.0269	0.1088 \pm 0.0243
	IMF2	0.124 \pm 0.0217	0.222 \pm 0.0226	0.1903 \pm 0.021	0.1034 \pm 0.0306
	IMF3	0.1116 \pm 0.032	0.2328 \pm 0.0231	0.1908 \pm 0.0268	0.0967 \pm 0.0449
	IMF4	0.1056 \pm 0.0373	0.2494 \pm 0.0664	0.227 \pm 0.02555	0.0922 \pm 0.0335
Thumb	IMF1	0.1331 \pm 0.0315	0.1963 \pm 0.0128	0.1546 \pm 0.0176	0.1061 \pm 0.025
	IMF2	0.1104 \pm 0.0334	0.1894 \pm 0.0297	0.1658 \pm 0.0169	0.0984 \pm 0.0329
	IMF3	0.1063 \pm 0.0168	0.1681 \pm 0.0251	0.1554 \pm 0.0166	0.1023 \pm 0.0281
	IMF4	0.0955 \pm 0.0239	0.1757 \pm 0.0125	0.1434 \pm 0.0367	0.0921 \pm 0.027
All fingers	IMF1	0.1405 \pm 0.0209	0.2477 \pm 0.0387	0.1662 \pm 0.018	0.1105 \pm 0.0173
	IMF2	0.1682 \pm 0.0247	0.2661 \pm 0.0171	0.1934 \pm 0.0209	0.136 \pm 0.0217
	IMF3	0.1753 \pm 0.026	0.2578 \pm 0.0241	0.2398 \pm 0.0305	0.1374 \pm 0.0258
	IMF4	0.155 \pm 0.02317	0.266 \pm 0.0204	0.2037 \pm 0.0243	0.1216 \pm 0.0222

Table 2
Parameters used in PIPE algorithm for architecture optimization of the neural tree.

Population size P_S	100
Elitist learning probability P_{el}	0.01
Learning rate l_r	0.01
Fitness constant	0.000001
Overall mutation probability P_M	0.4
Mutation rate m_r	0.4
Prune threshold T_p	0.999
Maximum random search steps	2000
Initial connection weights	rand $[-1, 1]$
Initial parameters a_p and b_p	rand $[0, 1]$

5. Results and discussions

The MLEs of original sEMG signals were shown in Table 3 whereas the MLEs of sEMG signals which were computed by using the method mentioned in Section 3.2 were shown in Table 4.

The classification accuracy (mean and standard deviation (SD)) of six hand gestures of the experiment is shown in Table 5 and Fig. 8.

From the above results (Table 5 and Fig. 8), it can be seen that the proposed nonlinear multiscale MLE model was able to classify six different hand gestures up to 97.6% accuracy. The method C (non-linear multiscale MLE method) outperforms the method A (MLE method) and method B (EEMD-based MLE method) algorithms. The current results show that better performance is obtained with the proposed scheme over the two previous techniques. The indicated accuracies have comparative values among the schemes.

Table 5

List of classification rates with different hand movements (Method A: MLE method, Method B: EEMD-based MLE method, Method C: nonlinear multiscale MLE method).

Hand gesture		Participants					Mean recognition rate \pm standard deviation
		Volunteer 1	Volunteer 2	Volunteer 3	Volunteer 4	Volunteer 5	
Ring finger	A	91.89%	80.59%	99.41%	92.76%	92.84%	91.50% \pm 1.1
	B	91.81%	94.44%	99.32%	90.07%	95.10%	94.15% \pm 0.9
	C	92.63%	95.25%	98.16%	93.12%	92.01%	94.23% \pm 0.2
Index finger	A	92.22%	83.3%	97.81%	88.96%	95.61%	91.58% \pm 1.2
	B	88.76%	90.10%	97.53%	92.20%	95.67%	92.85% \pm 0.8
	C	93.21%	91.50%	99.51%	92.66%	91.78%	93.73% \pm 0.3
Wrist	A	77.90%	89.66%	95.84%	93.12%	90.68%	89.44% \pm 0.9
	B	90.89%	88.58%	99.23%	92.86%	92.84%	92.88% \pm 0.78
	C	90.21%	92.64%	99.03%	89.77%	94.26%	93.18% \pm 0.25
Middle finger	A	87.80%	91.10%	99.30%	92.20%	96.70%	93.42% \pm 1.05
	B	96.04%	96.71%	99.32%	96.33%	98.32%	97.34% \pm 0.89
	C	96.23%	95.63%	98.95%	97.78%	98.52%	97.42% \pm 0.32
Thumb	A	81.19%	89.51%	98.90%	90.10%	91.41%	90.22% \pm 1.21
	B	89.76%	93.36%	95.81%	92.65%	89.37%	92.19% \pm 1.1
	C	90.56%	93.02%	98.71%	93.55%	89.83%	93.13% \pm 0.21
All fingers	A	91.67%	92.12%	98.78%	92.95%	92.83%	93.67% \pm 1.45
	B	94.63%	97.00%	99.36%	95.12%	94.71%	96.16% \pm 1.21
	C	95.92%	96.81%	99.62%	97.33%	98.21%	97.58% \pm 0.12

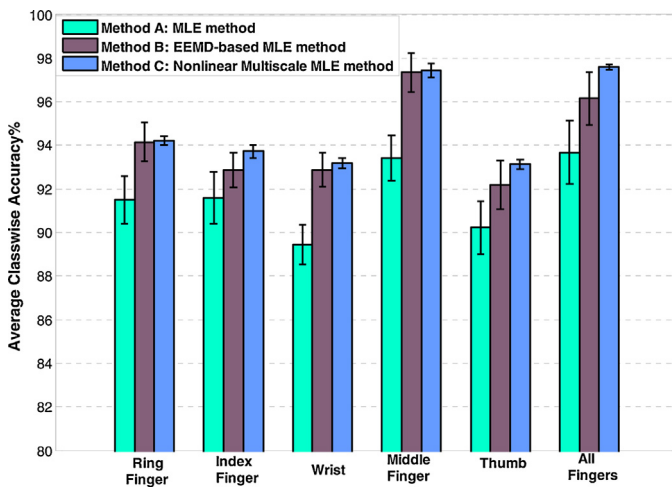


Fig. 8. Classification accuracy (%) mean and SD for the three methods.

From Tables 3 and 4 it can be seen that the mean and SD of nonlinear multiscale MLE values are higher for the original signals, whereas they are lower for the proposed method. Moreover, in order to improve the accuracy of FNT classifier the lower MLE values are essential. This is attributed to the best extracted nonlinear multiscale MLE features, which in turn provided higher classification accuracy.

Due to interference and cross-talk from adjacent muscles, it is understood that sEMG signals may demonstrate nonlinear characteristics for certain limb movement processes. This is evident from the literature where researchers cited about nonlinear (such as chaos) and high-dimension dynamics of sEMG signals [26]. Moreover, the proposed method is well suited for prosthetic applications and classification of complex hand movements where sEMG exhibits higher non-linearity.

Depending on the characteristics of the subject, it is possible to reach overall accuracy >95% for the recognition of 6 movements using fewer sensors. This result shows that training the proposed myoelectric control system it is possible to achieve better classification accuracy for several hand and finger movements. In particular, the proposed nonlinear multiscale MLE system could be applied in

a practical setting to make amputated subjects able to control hand and finger movements naturally.

6. Conclusions

In this paper, a hand gesture recognition method of sEMG based on nonlinear multiscale MLE and FNT is proposed. The nonlinear multiscale MLE method was adopted to extract features of sEMG signals and separate the main potential changes and these effects. FNT was used for hand gesture recognition based on feature values of sEMG signals. The study produced two important results.

The hand gesture recognition model, based on sEMG signals by using the nonlinear multiscale MLE method and FNT, is a novel sEMG signal action recognition model. It can adapt to the nonlinear and non-stationary characteristic of sEMG and can increase the classification accuracy of sEMG-based gestures. The nonlinear multiscale MLE method proved to be a good substitute for the EMD-based MLE method in bio-signal application as the former method can reduce dimensions of EMD decomposition automatically.

In conclusion, the nonlinear multiscale MLE method can obtain multiple characteristics of sEMG signal in the multiple scales and characterize the corresponding actions better. The FNT model is generated and evolved based on the pre-defined simple instruction sets, which can solve highly structure dependent problems of the ANN. The recognition model is able to classify six different hand gestures with higher classification accuracy. Future research will be to develop a real time myoelectric system based on the proposed scheme and test the robustness of the individual features such as electrode shift, electrode size and orientation, on amputees. Furthermore, the proposed technique could be tailored with more functional prosthetic arms using current machine learning approaches and most efficient rehabilitation programs.

References

- [1] M. Asghari Oskoei, H. Hu, Myoelectric control systems—a survey, *Biomed. Signal Process. Control* 2 (2007) 275–294.
- [2] W.S. Pease, H.L. Lew, *Johnson's Practical Electromyography*, Lippincott Williams & Wilkins, Ohio, 2007.
- [3] M. Lei, G. Meng, C. Jiaohui, Analysis of surface EMG signal based on empirical mode decomposition, in: *IEEE International Conference on Rehabilitation Robotics, 2009. ICORR'2009*, IEEE, 2009, pp. 230–233.

- [4] P. Padmanabhan, S. Puthusserypady, Nonlinear analysis of EMG signals-a chaotic approach, in: 26th Annual International Conference of the Engineering in Medicine and Biology Society, 2004. IEMBS'04, IEEE, 2004, pp. 608–611.
- [5] Y. Meng, B. Liu, Test nonlinear determinacy of electromyogram, in: 27th Annual International Conference of the Engineering in Medicine and Biology Society, 2005. IEEE-EMBS'2005, IEEE, 2006, pp. 4592–4595.
- [6] Q. Ai, Q. Liu, T. Yuan, Y. Lu, Gestures recognition based on wavelet and LLE, Australas. Phys. Eng. Sci. Med. (2013) 1–10.
- [7] P. Terrier, O. Dériaz, Kinematic variability, fractal dynamics and local dynamic stability of treadmill walking, J. Neuroeng. Rehabil. 8 (2011) 12.
- [8] R.B. Graham, E.M. Sadler, J.M. Stevenson, Local dynamic stability of trunk movements during the repetitive lifting of loads, Hum. Move. Sci. 31 (2012) 592–603.
- [9] K.P. Granata, S.A. England, Stability of dynamic trunk movement, Spine 31 (2006) E271.
- [10] M. Bask, R. Gençay, Testing chaotic dynamics via Lyapunov exponents, Physica D 114 (1998) 1–2.
- [11] Y. Guo, S. Huang, Y. Li, Single-mixture source separation using dimensionality reduction of ensemble empirical mode decomposition and independent component analysis, Circuits Syst. Signal Process. 31 (2012) 2047–2060.
- [12] B. Mijovic, M. De Vos, I. Gligorijevic, J. Taelman, S. Van Huffel, Source separation from single-channel recordings by combining empirical-mode decomposition and independent component analysis, IEEE Trans. Biomed. Eng. 57 (2010) 2188–2196.
- [13] N.E. Huang, M.L. Wu, W. Qu, S.R. Long, S.S. Shen, Applications of Hilbert–Huang transform to non-stationary financial time series analysis, Appl. Stoch. Models Bus. Ind. 19 (2003) 245–268.
- [14] I. Jolliffe, Principal Component Analysis, Wiley Online Library, 2002.
- [15] H. Abdi, L.J. Williams, Principal component analysis, Wiley Interdiscip. Rev.: Comput. Stat. 2 (2010) 433–459.
- [16] A. Wolf, J.B. Swift, H.L. Swinney, J.A. Vastano, Determining Lyapunov exponents from a time series, Physica D 16 (1985) 285–317.
- [17] S. Sato, M. Sano, Y. Sawada, Practical methods of measuring the generalized dimension and the largest Lyapunov exponent in high dimensional chaotic systems, Progr. Theor. Phys. 77 (1987) 1–5.
- [18] Y. Yu, L. Congming, W. Tingyu, Z. Xing, Fault diagnosis and classification for bearing based on EMD-ICA, in: International Conference on Electronic and Mechanical Engineering and Information Technology (EMEIT), 2011, IEEE, 2011, pp. 2715–2718.
- [19] W. Chen, Z. Wang, H. Xie, W. Yu, Characterization of surface EMG signal based on fuzzy entropy, IEEE Trans. Neural Syst. Rehabil. Eng. 15 (2007) 266–272.
- [20] A. Lemos, W. Caminhas, F. Gomide, Fuzzy evolving linear regression trees, Evol. Syst. 2 (2011) 1–14.
- [21] A.M. Silva, W. Caminhas, A. Lemos, F. Gomide, A fast learning algorithm for evolving neo-fuzzy neuron, Appl. Soft Comput. 14 (2014) 194–209.
- [22] Y. Chen, A. Abraham, B. Yang, Feature selection and classification using flexible neural tree, Neurocomputing 70 (2006) 305–313.
- [23] A. Abraham, H. Guo, H. Liu, Swarm intelligence: foundations, perspectives and applications, in: Swarm Intelligent Systems, Springer, 2006, pp. 3–25.
- [24] L. Cao, Practical method for determining the minimum embedding dimension of a scalar time series, Physica D 110 (1997) 43–50.
- [25] S. Xiaojing, T. Yantao, L. Yang, Feature extraction and classification of sEMG based on ICA and EMD decomposition of AR model, in: International Conference on Electronics, Communications and Control (ICECC), 2011, IEEE, 2011, pp. 1464–1467.
- [26] M. Lei, Z. Wang, Z. Feng, Detecting nonlinearity of action surface EMG signal, Phys. Lett. A 290 (2001) 297–303.